SHARAD radar sounding of the Vastitas Borealis Formation in Amazonis Planitia

Bruce Campbell,[1] Lynn Carter,[1] Roger Phillips,[2] Jeffrey Plaut,[3] Nathaniel Putzig,[2] Ali Safaeinili,[3] Roberto Seu,[4] Daniela Biccari,[4] Anthony Egan,[2] and Roberto Orosei[5]

Received 28 April 2008; accepted 3 November 2008; published 20 December 2008.

[1] Amazonis Planitia has undergone alternating episodes of sedimentary and volcanic infilling, forming an interleaved sequence with an upper surface that is very smooth at the kilometer scale. Earlier work interprets the near-surface materials as either young, rough lava flows or ice-rich sediment layers, overlying a basement comprising the Vastitas Borealis Formation and earlier Hesperian plains. Sounding radar profiles across Amazonis Planitia from the Shallow Radar (SHARAD) instrument on the Mars Reconnaissance Orbiter reveal a subsurface dielectric interface that increases in depth toward the north along most orbital tracks. The maximum depth of detection is 100–170 m, depending upon the real dielectric permittivity of the materials, but the interface may persist at greater depth to the north if the reflected energy is attenuated below the SHARAD noise floor. The dielectric horizon likely marks the boundary between sedimentary material of the Vastitas Borealis Formation and underlying Hesperian volcanic plains. The SHARAD-detected interface follows the surface topography across at least one of the large wrinkle ridges in north central Amazonis Planitia. This conformality suggests that Vastitas Borealis sediments, at least in this region, were emplaced prior to compressional tectonic deformation. The change in radar echo strength with time delay is consistent with a loss tangent of 0.005–0.012 for the column of material between the surface and the reflector. These values are consistent with dry, moderate-density sediments or the lower end of the range of values measured for basalts. While a component of distributed ice in a higher-loss matrix cannot be ruled out, we do not find evidence for a dielectric horizon within the Vastitas Borealis Formation that might suggest an abrupt change from an upper dry layer to an ice-rich lower deposit.

Citation: Campbell, B., L. Carter, R. Phillips, J. Plaut, N. Putzig, A. Safaeinili, R. Seu, D. Biccari, A. Egan, and R. Orosei (2008), SHARAD radar sounding of the Vastitas Borealis Formation in Amazonis Planitia, *J. Geophys. Res.*, *113*, E12010, doi:10.1029/2008JE003177.

1. Introduction

[2] Amazonis Planitia, a lowland plains region roughly 1300 km × 900 km, is located immediately north of the hemispheric dichotomy boundary and west of the massive Tharsis volcanic complex. This region (Figure 1) has undergone a sequence of geologic events whose relative timing and association with water are not fully understood. Possibly formed by an impact [*Fuller and Head*, 2002] after the development of the dichotomy boundary, the basin was resurfaced with Hesperian plain units and materials of the Vastitas Borealis Formation (VBF). The Arcadia Planitia component of the Hesperian plains, unit HAa of *Tanaka et al.* [2005], is likely flood lavas, but the Vastitas Borealis Formation has been attributed to sedimentary infilling of the northern lowlands, perhaps in the presence of large bodies of water [e.g., *Tanaka and Scott*, 1987; *Clifford and Parker*, 2001; *Kreslavsky and Head*, 2002]. *Tanaka et al.* [2005] use the deposition of the Vastitas Borealis Formation (their units ABvi and ABvm) to mark the beginning of the Amazonian period, in contrast to earlier work that considered it to be of late Hesperian age. Remnant Noachian materials form the Erebus Montes and small outcrops along the highland margin (Figure 2).

[3] *Fuller and Head* [2002] and *Tanaka et al.* [2005] suggest that an early Amazonian phase of volcanism associated with Olympus Mons formed a hummocky, extensive deposit (unit AAa1n) across northern Amazonis Planitia. Subsequent gravity sliding in the middle Amazonian covered the eastern part of this unit with Olympus Mons aureole deposits (unit Atl). A middle Amazonian unit (AAa2n) forms the very smooth (at a scale of hundreds of meters to a few kilometers) central region of Amazonis

[1] Center for Earth and Planetary Studies, Smithsonian Institution, Washington, D. C., USA.
[2] Southwest Research Institute, Boulder, Colorado, USA.
[3] Jet Propulsion Laboratory, Pasadena, California, USA.
[4] INFOCOM, University of Rome "La Sapienza," Rome, Italy.
[5] Istituto di Astrofisica Spaziale e Fisica Cosmica, Rome, Italy.

Copyright 2008 by the American Geophysical Union.
0148-0227/08/2008JE003177

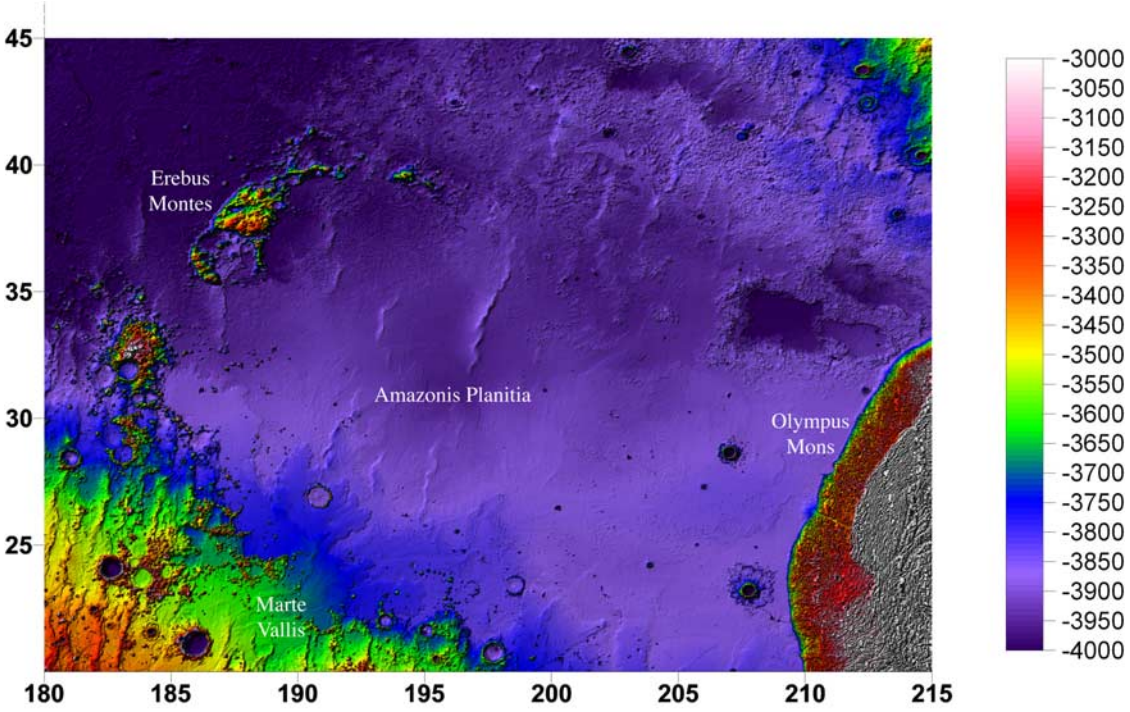

Figure 1. Geographic features of Amazonis Planitia labeled on color shaded relief MOLA data. Simple cylindrical map projection for the region 20°N–45°N, 180°E–215°E. Color scale indicates differences in meters from reference ellipsoid.

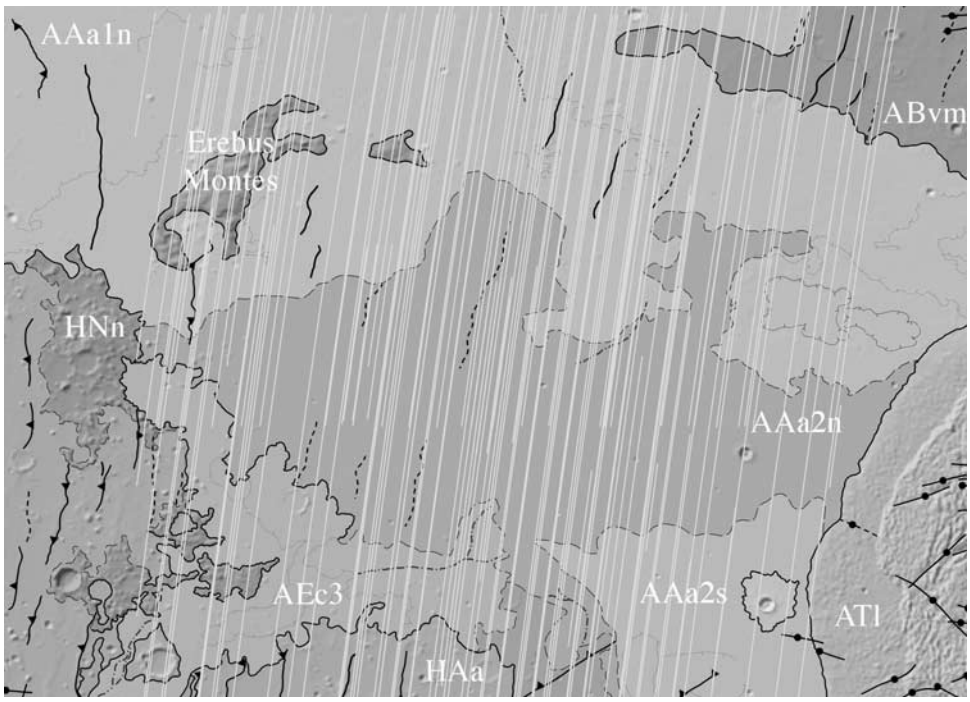

Figure 2. A portion of the geologic map of *Tanaka et al.* [2005] for Amazonis Planitia, with SHARAD ground tracks indicated by light gray lines. Simple cylindrical map projection for the region 20°N–45°N, 180°E–215°E. Unit abbreviations correspond to Noachian uplands (HNn), Hesperian plains (HAa), the Vastitas Borealis Formation (ABvm), portions of the Olympus Mons deposits (AAa1n and ATl), middle Amazonian materials (AAa2n and AAa2s), and later Amazonian lobate materials (Aec3). Small portion of early Amazonian–late Hesperian volcanic or debris flows (AHAa1s) is at lower center.

Planitia and is suggested by *Tanaka et al.* [2005] to be dominated by lava flows, with possible postemplacement modification by water-carved channels [*Fuller and Head*, 2002].

[4] A final pulse of volcanic activity from the Cerberus Fossae region [*Plescia*, 1990] emplaced lobate features a few tens of meters in height along the highlands margin in southern Amazonis (unit AEc3). In high-resolution photos, these have similar morphology to the rafted platy structure of terrestrial flood basalts [*Keszthelyi et al.*, 2000]. A second interpretation suggests that the putative lava flows are ice-rich units, similar to modern circumpolar polygonal-patterned ground, presently undergoing sublimation loss [*Page*, 2007]. The interpretation of the platy structure in areas of Elysium Planitia as the surface signature of flood-like lava flows has also been challenged by *Murray et al.* [2005], who propose that these landforms reflect the surface of a frozen body of water, with the possibility of remnant ice at some depth beneath the surface.

[5] In this paper, we use radar sounder data from the Shallow Radar (SHARAD) instrument on the Mars Reconnaissance Orbiter (MRO) to provide a first look beneath the surface of Amazonis Planitia. SHARAD uses a 15–25 MHz signal to penetrate hundreds of meters into dry geologic materials [*Seu et al.*, 2007a, 2007b]. The transmitted low-power (10-W) signal is swept over a range of frequencies in a long (85-μs) pulse that is compressed in time upon reception. The effective free space vertical resolution of the received signals is about 15 m; in geologic materials this resolution improves as the inverse square root of the real dielectric constant. Most near-surface dry materials have dielectric constants of 3–8, so the vertical resolution is 5–9 m. However, the use of a chirped signal creates sidelobes in the range-compressed echoes that can obscure shallow subsurface reflections (within ~30–50 m of the surface). The horizontal footprint of the received echoes is improved in the along-track direction to about 500 m by focused Doppler processing and is a few kilometers across track, depending upon the roughness of the surface. Echoes from off-nadir surface topography (clutter) can obscure reflections from subsurface interfaces or create spurious features that may appear to arise in the subsurface. Surface clutter echoes are identified, in part, by creating simulated sounder echo profiles on the basis of Mars Orbiter Laser Altimeter (MOLA) topography [*Smith et al.*, 2001] although the coarse spatial sampling of these data means that smaller surface features (hills and craters) may not be represented. The effects of the Mars ionosphere are relatively small for the nighttime observations used here, so no frequency-dependent correction was necessary to compensate for distortion of the chirped signal.

[6] Section 2 reviews the basic properties of Amazonis Planitia revealed by orbital remote sensing and Earth-based radar mapping. Section 3 presents the SHARAD data for this region and the inferred thickness and extent of deposits above a widespread dielectric interface. We also show that the correlation of this subsurface interface with the surface topography of wrinkle ridges serves to constrain the likely stratigraphy and the relative timing of deformation. Section 4 analyzes the variation in echo power with the depth of the interface below the surface to derive an estimate for the electrical loss properties. Section 5 discusses the geological implications of our results.

2. Topography and Near-Surface Roughness of Amazonis Planitia

[7] The central portion of Amazonis Planitia (unit AAa2n of *Tanaka et al.* [2005]) is the smoothest large region on Mars at horizontal scales of a few tens of meters and larger, as evidenced by the low roughness value in all three horizontal-scale ranges derived from the MOLA topography data by *Kreslavsky and Head* [1999, 2000]. This region also has a high degree of modeled surface dust coverage, a low thermal inertia consistent with extensive surface dust and minimal exposed rock, and generally modest albedo and color contrasts [*Ruff and Christensen*, 2002; *Putzig et al.*, 2005]. An earlier northern Amazonian flow unit (AAa1n) is considerably more rugged, indicating some difference in its emplacement or modification history from the smoother materials in the central basin [*Tanaka et al.*, 2005]. Marte Vallis apparently served as a source channel for materials (lava flows and/or water-transported sediments) that debouched into the basin to form lobate features about 30 m thick (Figure 1, unit AEc3). Areas farther into the central basin (unit AAa2n) are much more muted in morphology. This shift in surface relief may reflect a change in materials or emplacement regime from the lobe-forming deposits emerging from the highlands or increasing coverage of the surface by fine-grained materials.

[8] The basin topography is also marked by a roughly N–S trending suite of wrinkle ridges a few tens of meters in maximum relief (Figure 1), which appear similar to ridges formed in highland terrain to the south and lowland plains to the north of Amazonis Planitia [e.g., *Plescia*, 1993]. The timing of wrinkle ridge formation is uncertain. *Fuller and Head* [2002] and *Head et al.* [2002] suggest that the ridges formed only in the early Hesperian plains materials and are, thus, muted by the Vastitas Borealis Formation, whereas *Tanaka et al.* [2005] leave open the possibility of continuing deformation through the early Amazonian period.

[9] Earth-based radar mapping provides a unique view of near-surface dielectric and roughness properties. Images collected using the Arecibo Observatory 12.6-cm radar system have a spatial resolution of ~30 km but are sensitive to variations in surface height statistics at scales of 2 cm and larger and to rocks of this size range on the surface or within the probing depth of the radar (about a meter). Because of the rapid spin rate of Mars, special techniques must be used to form high-resolution images, and the best quality is obtained for the same sense circular ("depolarized") echo polarization. Radar data collected in 1992–1993 (Figure 3) show a high-backscatter region comprising south central and southern Amazonis Planitia and extending through Marte Vallis into Elysium Planitia [*Harmon et al.*, 1999]. These and other authors suggest that the contiguous high-backscatter signatures across Elysium Planitia, Marte Vallis, and Amazonis Planitia indicate broad coverage by rough lava flows from Cerberus Fossae, with areas farther into Amazonis mantled by a meter or so of dust that mutes the visible surface morphology [*Harmon et al.*, 1999; *Keszthelyi et al.*, 2000; *Tanaka et al.*, 2005]. An alternate view proposes that these platy textures are indicative of ice-rich ground

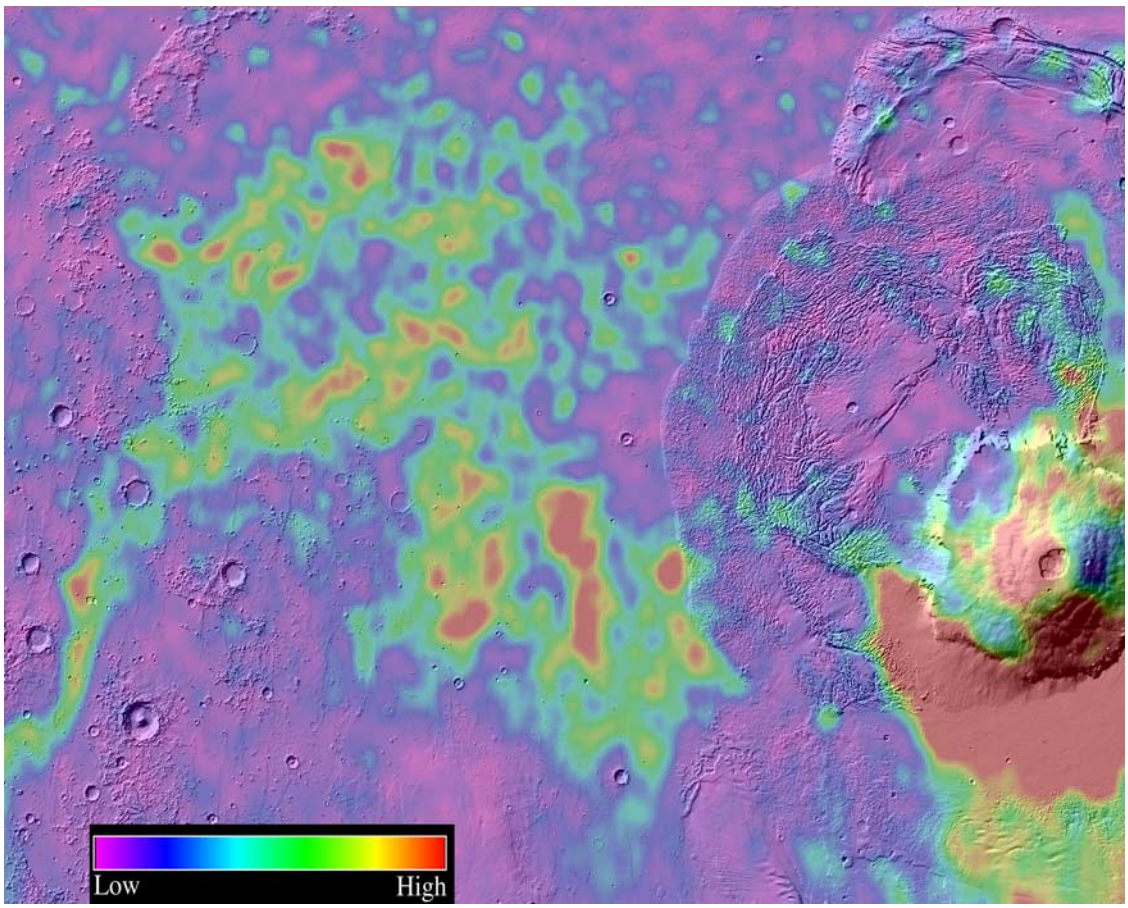

Figure 3. Earth-based 12.6-cm radar backscatter data for Amazonis Planitia, overlaid as color on shaded relief base. Data are from *Harmon et al.* [1999]. Area covered 5°N–40°N, 180°E–230°E. Color bar indicates scaling from low to high radar reflectivity. Note the high-backscatter signatures of lava flows south of Olympus Mons and in a fan-like pattern extending from Marte Vallis (lower left) northeastward into Amazonis Planitia.

[*Murray et al.*, 2005] and perhaps of extant ground ice in midlatitude deposits [*Page*, 2007].

3. SHARAD Mapping of Subsurface Dielectric Horizons

[10] SHARAD data are presented here as "radar grams" showing the variations in echo strength with time delay assembled along the spacecraft ground track for each orbit. The principal sources of reflected signal are smooth regions of the surface that face toward the sensor and similarly smooth subsurface interfaces. In rugged terrain, there may be significant clutter echoes that arise from sloping features located to either side of the nadir track, such as crater walls or wrinkle ridges. Within Amazonis Planitia, the clutter-producing features are primarily impact craters.

[11] SHARAD observations across Amazonis Planitia reveal the widespread occurrence of a single subsurface interface (Figures 4 and 5) at round-trip time delays as great as 1.95 μs after the surface echo. In some orbit tracks, this reflecting horizon is horizontally continuous over hundreds of kilometers, while in others the subsurface echoes are segmented, sometimes interrupted by surface features such as impact craters. In all cases, the detected horizon is either at a constant depth (time delay) or occurs at greater depth toward the north in each track. The shallower echoes are typically lost in the sidelobe pattern of the surface echo when the two reflections are less than about 0.6 μs apart. The northern extent of this reflecting horizon appears to be controlled by greater attenuation with increasing depth below the surface, aggravated by increasing surface clutter due to hummocky and hilly terrain in the north part of the basin, and it is likely that the interface continues beyond the limits mapped by SHARAD. Supporting this hypothesis is the fact that in some orbit tracks, the SHARAD SNR is better because of more favorable positioning of the MRO solar panels and/or high-gain antenna, and in these tracks we observe a deeper, more northward extension of the reflector into the region of increased surface clutter (Figure 5). Taken together, the numerous SHARAD profiles across the basin reveal the general topography of the subsurface dielectric interface (Figure 6).

[12] The depth to the reflecting horizon, h, is related to the round-trip delay time, Δt, and the depth-averaged value of the real permittivity, ε', of materials between the surface and the interface:

$$h = \frac{\Delta t c}{2\sqrt{\varepsilon'}}, \tag{1}$$

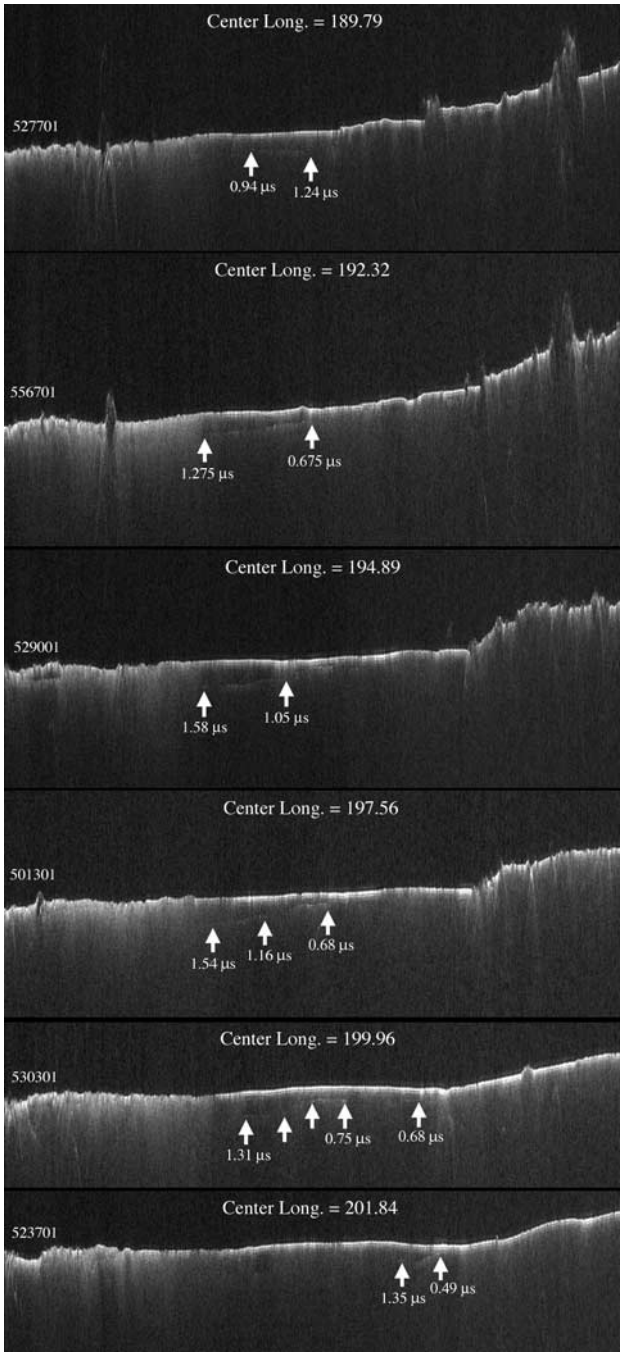

Figure 4. SHARAD radargrams for six orbit tracks over Amazonis Planitia. The longitude of the center point of each track is labeled. On each radargram, left is toward the N–NE and right is toward the S–SW, extending about 1765 km along track from 44.7°N–14.9°N. White arrows denote a subsurface reflector at the noted round-trip travel time with respect to the surface echo.

where c is the speed of light in a vacuum. The range in ε' for dry geologic materials is relatively narrow, from about 3 for ice and poorly consolidated sediments to 8 for dense igneous material [*Ulaby et al.*, 1988; *Carrier et al.*, 1991]. Over this range, the conversion factor for reflector depth is 53 ($\varepsilon' = 8$) to 87 m ($\varepsilon' = 3$) per microsecond of round-trip delay.

[13] An important aspect of the correlation between the subsurface reflecting horizon and regional stratigraphy is revealed by SHARAD sounding tracks (Figure 5) that cross a large wrinkle ridge (Figures 2 and 6) in the north central part of Amazonis Planitia. The reflecting horizon follows the topographic variations of the ridge and is continuous beneath this structure, showing that materials above and below the dielectric interface were folded during ridge formation. The surface radar echo power decreases over the ridge, so roughness at scales comparable to the SHARAD wavelength may be greater on the exposed ridge terrain than in the nearby plains (though local slopes of a few degrees could also diminish these returns).

4. Analysis of Dielectric Loss Properties

[14] Natural materials have electrical properties that vary with composition, mineralogy, density, temperature, and the frequency of the probing signal. Where they can be derived from the sounder data, the apparent values of the real permittivity and the attenuation (or loss tangent) can be compared to results from laboratory studies of lunar and terrestrial materials. In general, strong constraints on the real dielectric constant from sounder echoes can be obtained only where the depth of a reflecting interface can be determined from other data, such as the assumption of relatively horizontal plain surfaces beneath the Medusae Fossae Formation by *Watters et al.* [2007]. In an idealized plane-layered scenario, we could also use the relative strength of the surface and subsurface echoes to constrain the sense of the dielectric contrast at an interface (e.g., low-density to high-density material or vice versa). For the Amazonis Planitia data, however, additional unknown factors, such as the depth and variability of surface dust cover, make this type of analysis impractical.

[15] The loss tangent may be estimated from variations in radar echo strength with greater time delay relative to the surface echo, under a specific set of constraints. If (1) the surface roughness at the SHARAD wavelength scale is

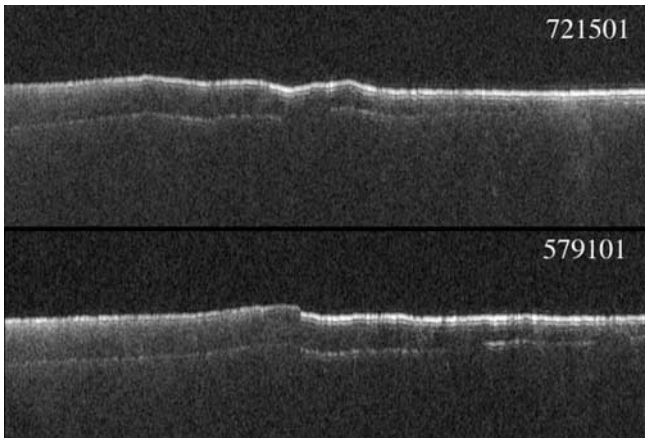

Figure 5. Portions of two SHARAD radargrams for tracks that cross wrinkle ridges (about 60 m in maximum relief) in north central Amazonis Planitia (see Figures 2 and 6). North is toward the left; image width is about 315 km. Note that the subsurface reflecting horizon parallels the topography of the ridge and is continuous beneath this structure.

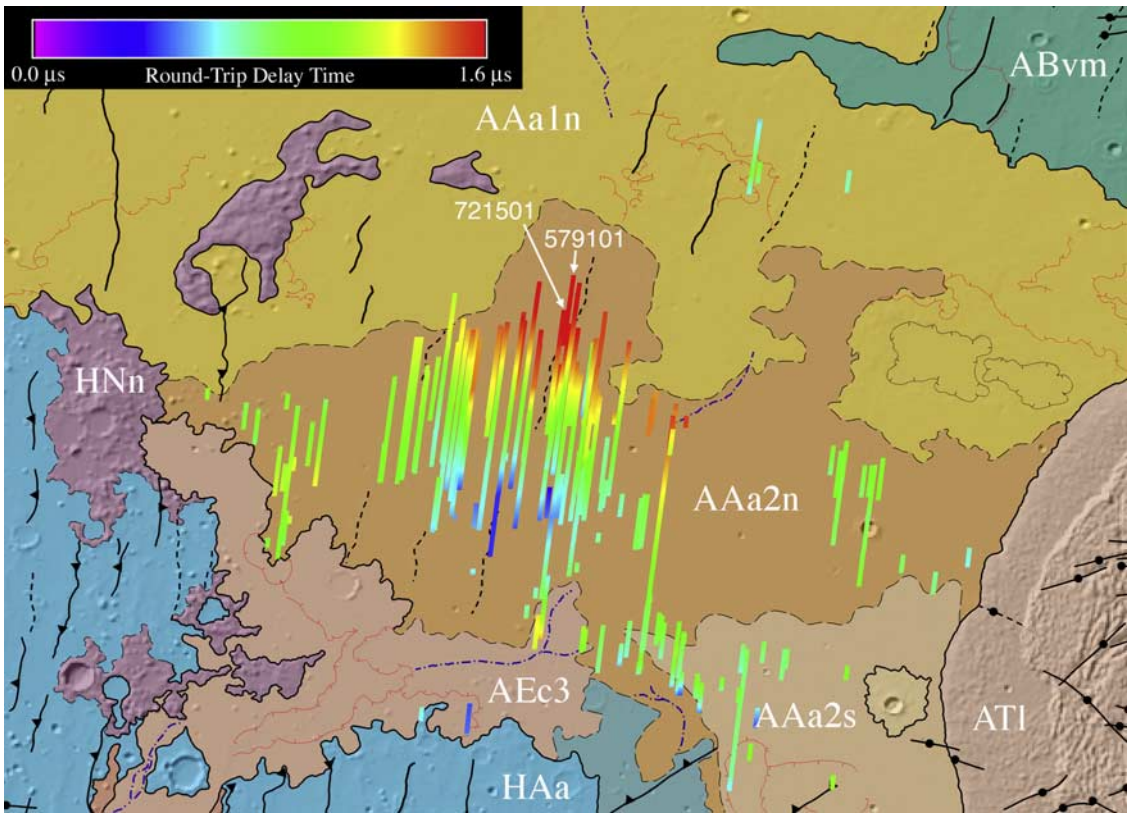

Figure 6. SHARAD subsurface reflections presented as color overlay for variations in round-trip echo delay on a portion of the geologic map by *Tanaka et al.* [2005]. Simple cylindrical map projection for the region from 20°N to 45°N, 180°E to 215°E.

constant with respect to position, (2) the subsurface interface also has constant roughness on the scale of the radar wavelength in the medium, (3) the probed layer has constant dielectric loss properties, and (4) the real dielectric contrasts at the surface-atmosphere and subsurface interfaces are constant over some length of the detected interfaces, then any observed changes in the backscattered subsurface power are dependent only upon the thickness of the layer being probed [cf. *Porcello et al.*, 1974; *Watters et al.*, 2007].

[16] The complex permittivity of a material is given by $\varepsilon' + i\varepsilon''$. The loss tangent, $\tan\delta = \varepsilon''/\varepsilon'$, is related to the signal attenuation in the medium as a function of distance traveled. The basic observations of the subsurface interface provide a measure of round-trip power loss as a function of time delay with respect to the surface echo (in μs). For a starting amount of power given by P_o, the remaining power in the wave after some distance traveled, x, through a lossy medium is

$$P(x) = P_o \exp\left[\frac{-4\pi x}{\lambda}\sqrt{\frac{\varepsilon'}{2}\left(\sqrt{1+\tan^2\delta}-1\right)}\right], \qquad (2)$$

where λ is the free space radar wavelength (15 m for the SHARAD center frequency) [*Ulaby et al.*, 1982]. If we assume round-trip travel ($x = 2h$), the observed power loss is

$$L = \frac{P(h)}{P_o} = \exp\left[\frac{-8\pi h}{\lambda}\sqrt{\frac{\varepsilon'}{2}\left(\sqrt{1+\tan^2\delta}-1\right)}\right]. \qquad (3)$$

Combining (1) and (3), the apparent loss tangent is related to the observed power loss, L, for some time delay, Δt, as

$$\tan\delta = \sqrt{\left\{2\left[\frac{\lambda}{4\pi c\Delta t}\ln(L)\right]^2+1\right\}^2-1}. \qquad (4)$$

[17] We determined a best fit power loss (in dB/μs) for echoes along four sloping SHARAD-detected interfaces (Figure 7, Table 1). We subtract the average echo power for the surface above the studied horizon, so the vertical axis in each plot represents differences with respect to this reference reflection. Taking one standard deviation about the derived value of the slope, and converting the decibel values to a linear format prior to using (4), we obtain a range of loss tangent of 0.005–0.012.

5. Geologic Interpretation

[18] The subsurface interfaces detected by SHARAD across much of southern and central Amazonis Planitia likely represent a density contrast between two geologic deposits. Such a density contrast could arise from the juxtaposition of dense lava flows and less dense sediments or from the presence of a thin (of the order of 1 m) soil deposit between two layers of similar density, as observed for mare basalts on the Moon [*Peeples et al.*, 1978]. The maximum thickness of materials above the reflector is 100 ($\varepsilon' = 8$) to 170 m ($\varepsilon' = 3$), on the basis of a maximum round-

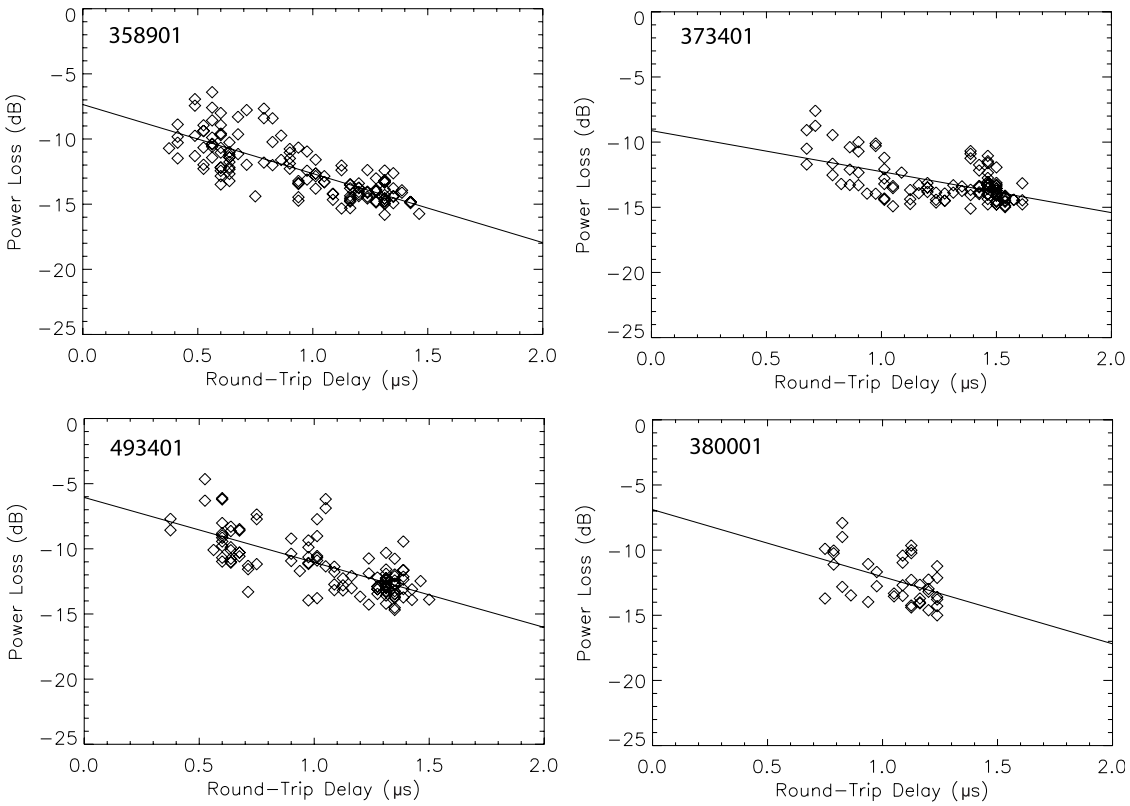

Figure 7. SHARAD subsurface reflector power loss (in dB) versus round-trip time delay for orbit tracks over Amazonis Planitia. Power values are normalized to the average of surface echo power along each track and fit with a simple power law (straight lines). See Table 1 for best fit slope values.

trip delay of ~1.95 μs. We do not observe additional shallower layering in the SHARAD echoes but cannot discriminate vertical structure within about 30–50 m (~0.6 μs round-trip delay) of the surface echo because of its sidelobe pattern.

[19] The lateral extent of the detected interface along any given orbit track generally correlates with the mapped middle Amazonian units AAa2n and AAa2s of *Tanaka et al.* [2005] (Figure 6). From a few tracks with exceptional SNR, we see the reflecting horizon persist a modest distance beneath more rugged (higher-clutter) terrain in the north part of the basin (Figure 5), but only rarely do these interfaces cross the mapped boundary with the proto-Olympus flow unit AAa1n. To the west, another group of detections again suggests a gradual increase in reflector depth toward the north. These detections are more widely spaced in longitude because of the smaller number of SHARAD tracks acquired for this region (Figure 2) and do not persist as far north into the mapped AAa2n unit as those of the central basin. We observe the same type of shallow reflections along the highland boundary toward the east (Figure 6), some of which extend into the southern flow unit AAa2s. There are only a few orbit tracks with interface detections in the east central part of Amazonis Planitia, however, and these occur at a nearly constant, relatively shallow depth below the surface. This change in the detected reflections is paralleled by a reduction from west to east in the population of wrinkle ridges that deform the basin-filling material [*Fuller and Head*, 2002; *Tanaka et al.*, 2005].

[20] On the basis of previous geologic mapping, the post-Noachian stratigraphy of central Amazonis Planitia is characterized by, from lowest to highest, (1) Hesperian plains of the Arcadia Planitia unit, (2) materials of the VBF, (3) some possible gradational thickness of the proto-Olympus flow unit present at the surface to the north (AAa1n) [*Fuller and Head*, 2003], and (4) the southern and northern mid-Amazonian flow units AAa2s and AAa2n [*Tanaka et al.*, 2005]. The reflecting horizons in this central region could thus arise from either the Hesperian plains-VBF interface or the contacts between the VBF and the two overlying units. We propose, for reasons described below, that the Hesperian plains-VBF scenario best fits the SHARAD observations (e.g., Figure 8a) and the inferred stratigraphy (Figure 8b).

[21] First, the SHARAD-detected interfaces in western and central Amazonis Planitia are consistent with a single, gently north dipping geologic interface. If the VBF materials

Table 1. Loss Properties and Model-Derived Loss Tangents for Amazonis Planitia Deposits

Track	Intercept (dB)	Slope (dB/μs)	SD of Slope	Loss Tangent[a]
358901	−7.35	−5.30	0.38	0.009–0.010
373401	−9.12	−3.15	0.46	0.005–0.007
493401	−6.06	−4.98	0.46	0.008–0.010
380001	−6.89	−5.15	1.60	0.007–0.012

[a]Range of loss tangents reflects the range of the slope for ±1 standard deviation about the best fit values taken from Figure 7.

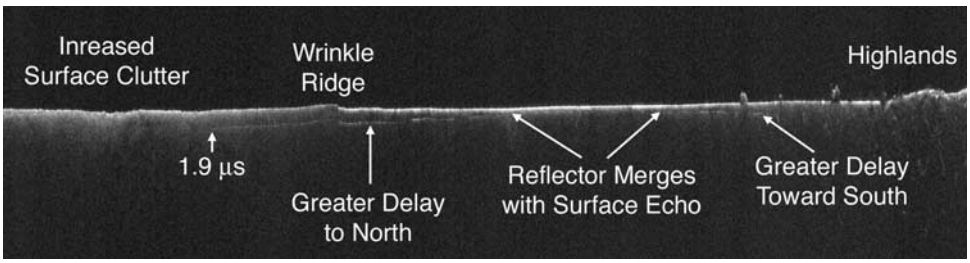

Figure 8a. SHARAD radar data for orbit track 579101. North is toward the left, and radargram width is about 1150 km. The location of track 579101 is noted on Figure 6.

formed as sediments from outflow events and/or the remnants of a northern ocean, we would expect a nearly equipotential surface to result. The observed gradient is thus more likely to be the Hesperian plains sloping away from the highlands dichotomy boundary. Second, the estimated thickness range of the deposits between the surface and the reflector matches that based on models for the VBF thickness from channel discharge volumes and stratigraphic studies [*Kreslavsky and Head*, 2002]. Third, the decreasing reflector depth toward the south is consistent with outcrops of the Arcadia Planitia unit (HAa) of Hesperian plains along the southern margin of Amazonis Planitia (Figure 6) [*Tanaka et al.*, 2005].

[22] In this scenario, the similarity in relief between the subsurface reflector and the surface topography over at least one major wrinkle ridge in central Amazonis Planitia would imply concurrent folding of both the Hesperian plains and the VBF materials. *Tanaka et al.* [2005] suggest that some degree of compressional deformation continued into the early to middle Amazonian, affecting the VBF, which is consistent with the SHARAD observations. This correspondence is in contrast to studies concluding that undeformed VBF widely superposes early Hesperian wrinkle ridges [e.g., *Head et al.*, 2002]. Perhaps this relationship between sedimentation and tectonism is unique to western and central Amazonis Planitia.

[23] Alternative models for the geologic contact linked with the central Amazonis SHARAD reflector raise significant issues of process and timing. If the radar-detected interface were stratigraphically lower (e.g., a soil horizon between major pulses of Hesperian plains–forming volcanism), our overall model for emplacement and deformation of the VBF would not change, but the total implied volume of material above the plains basement would decrease. If the interface is higher in the column (e.g., the contact between the top of the VBF and the overlying volcanic flows or sediments), it is difficult to explain an interface that slopes upward toward the south for VBF material from a northern source. This scenario also requires that compressional deformation to form the major wrinkle ridges be even later in time than proposed by *Tanaka et al.* [2005] since the layer above the radar-detected interface (some combination of AAa1n and AAa2n in this model) is also folded.

[24] The abrupt shift in the nature and distribution of the SHARAD-detected interfaces between central and eastern Amazonis Planitia has little apparent correlation with the mapped geology, except to the extent that wrinkle ridge structures are less pronounced in the eastern part of the basin. If our model is correct, then the gap in subsurface radar reflections suggests an absence of the strong density contrast associated with the plains-VBF horizon. A possibility is that the Hesperian plains beneath east central Amazonis are topographically higher by a few tens of meters or superposed by early lava flows, such that VBF materials simply embay the flanks of this uplift or flow complex. The absence of SHARAD reflections would thus be due to the lack of a strong density contrast between the plains- or complex-forming lavas and later basin-filling

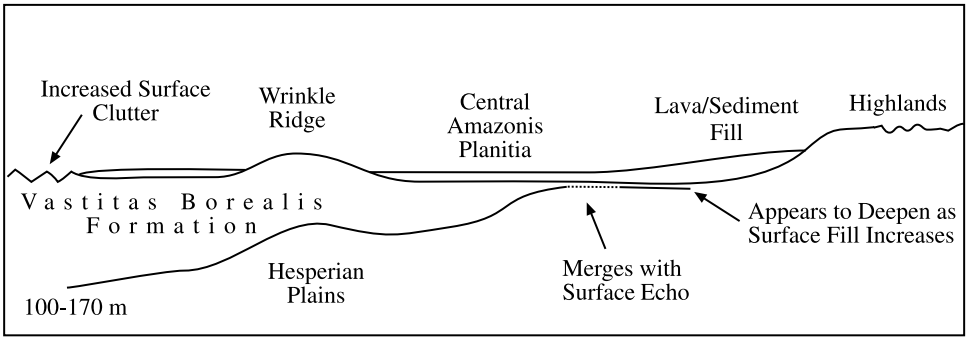

Figure 8b. Cartoon of inferred stratigraphy along SHARAD track shown in Figure 8a. Depth ranges are based on observed round-trip delay and possible range of real dielectric constant (larger depth values assume a real dielectric constant of 3; smaller values assume a real dielectric constant of 8); vertical scale is exaggerated. Note that a shallow and (we infer) near-horizontal portion of the reflecting horizon appears to deepen (greater round-trip time delay in Figure 8a) toward the south as the surface topography increases onto lobate flow features at the basin margin.

units (AAa1n and AAa2n). Alternatively, there may be one or more rugged (on a several-meter scale) interfaces between units in the upper 50–100 m of eastern Amazonis that greatly limit penetration by the SHARAD signals. The decrease in wrinkle ridges toward the east may favor the former explanation, suggesting a difference in the time sequence of basin folding and infilling.

[25] Assuming that our preferred model for the radar-observed stratigraphy is correct, SHARAD data offer some insight into the nature of materials above the Vastitas Borealis deposit. *Fuller and Head* [2002] and *Tanaka et al.* [2005] postulate flooding of the basin by lava flows and water-borne sediments during the Amazonian period, so these materials contribute to some depth of fill above the VBF. Earth-based radar data suggest a surface geologic unit across Amazonis Planitia with rugged centimeter- to meter-scale morphology [*Harmon et al.*, 1999], while optical and thermal infrared data clearly show a mantle of dust. The primary conclusion with regard to these potentially interleaved fluvial and volcanic events is that the total depth of fill above the VBF either does not exceed the apparent depth of the surface sidelobes (30–50 m) or has little dielectric contrast with the underlying materials. The former explanation seems most plausible, even if only on the basis of volume considerations for materials distributed over such a large area.

[26] One outstanding question regarding the Vastitas Borealis Formation is whether ice-rich deposits may be preserved beneath dry sediment cover. *Kreslavsky and Head* [2002] argue that such an ice deposit, while postulated by others as a remnant of large-scale flooding and formation of an insulating cap [e.g., *Clifford and Parker*, 2001], is not present below the relatively thin (~100 m) VBF that they infer from studies of stratigraphy and topographic variations. Our SHARAD mapping of VBF materials as <170 m thick across Amazonis Planitia is consistent with this hypothesis. In addition, we observe no additional dielectric layering as the VBF increases in thickness toward the north, as might be expected if an ice-rich layer were present only under the deeper portions of a cap material.

[27] Could there be residual ice as a distributed component within the VBF rather than as a discrete body at depth? The derived microwave loss properties reflect the depth-averaged properties of the column of material above the Hesperian plains basement. The estimated values of 0.005–0.012 are low compared to some terrestrial basalts but are consistent with lunar basalts [*Carrier et al.*, 1991] and with other basalt samples measured at very low atmospheric pressure. Given that we expect the VBF to be a sedimentary unit of lower density than that of typical basalt, there seems little need to invoke a significant fraction of low-loss ice to explain the observations. Nevertheless, the SHARAD data cannot be used to rule out the presence of ice, especially at a low-volume fraction, within a matrix of higher-loss material.

[28] **Acknowledgments.** We thank the SHARAD Operations Center team, including Emanuele Giacomoni, Federica Russo, Marco Cutigni, Oreste Fuga, and Riccardo Mecozzi, for their efforts in targeting the observations and ensuring that the best possible data are obtained with the instrument. Fabrizio Bernardini provided invaluable assistance in processing the data and making them accessible to the science team. We also thank the SHARAD and MRO engineering and operations teams for their work in building and operating the equipment. SHARAD was provided by the Italian Space Agency through a contract with Thales Alenia Space Italia, and it is operated by the INFOCOM Department, University of Rome. Reviews by J. K. Harmon and an anonymous referee were very helpful in revising the manuscript.

References

Carrier, W. D., G. R. Olhoeft, and W. Mendell (1991), Physical properties of the lunar surface, in *Lunar Sourcebook*, edited by G. Heiken, D. Vaniman, and B. M. French, pp. 475–594, Cambridge Univ. Press, New York.

Clifford, S. M., and T. J. Parker (2001), The evolution of the Martian hydrosphere: Implications for the fate of a primordial ocean and the current state of the northern plains, *Icarus*, *154*, 40–79, doi:10.1006/icar.2001.6671.

Fuller, E. R., and J. W. Head III (2002), Amazonis Planitia: The role of geologically recent volcanism and sedimentation in the formation of the smoothest plains on Mars, *J. Geophys. Res.*, *107*(E10), 5081, doi:10.1029/2002JE001842.

Fuller, E. R., and J. W. Head III (2003), Olympus Mons, Mars: Detection of extensive preaureole volcanism and implications for initial mantle plume behavior, *Geology*, *31*(2), 175–178, doi:10.1130/0091-7613(2003)031<0175:OMMDOE>2.0.CO;2.

Harmon, J. K., R. E. Arvidson, E. A. Guinness, B. A. Campbell, and M. A. Slade (1999), Mars mapping with delay-Doppler radar, *J. Geophys. Res.*, *104*, 14,065–14,089, doi:10.1029/1998JE900042.

Head, J. W., III, M. A. Kreslavsky, and S. Pratt (2002), Northern lowlands of Mars: Evidence for widespread volcanic flooding and tectonic deformation in the Hesperian Period, *J. Geophys. Res.*, *107*(E1), 5003, doi:10.1029/2000JE001445.

Keszthelyi, L., A. S. McEwen, and T. Thordarson (2000), Terrestrial analogs and thermal models for Martian flood lavas, *J. Geophys. Res.*, *105*, 15,027–15,049, doi:10.1029/1999JE001191.

Kreslavsky, M. A., and J. W. Head III (1999), Kilometer-scale slopes on Mars and their correlation with geologic units: Initial results from Mars Orbiter Laser Altimeter (MOLA) data, *J. Geophys. Res.*, *104*, 21,911–21,924, doi:10.1029/1999JE001051.

Kreslavsky, M. A., and J. W. Head III (2000), Kilometer-scale roughness on Mars: Results from MOLA data analysis, *J. Geophys. Res.*, *105*, 26,695–26,711, doi:10.1029/2000JE001259.

Kreslavsky, M. A., and J. W. Head (2002), Fate of outflow channel effluents in the northern lowlands f Mars: The Vastitas Borealis Formation as a sublimation residue from frozen ponded bodies of water, *J. Geophys. Res.*, *107*(E12), 5121, doi:10.1029/2001JE001831.

Murray, J. B., J.-P. Muller, G. Neukum, E. Hauber, W. J. Markiewicz, J. W. Head, B. H. Foing, D. P. Page, K. L. Mitchell, and G. Portyankina (2005), Evidence from the Mars Express High Resolution Stereo Camera for a frozen sea close to Mars' equator, *Nature*, *434*, 352–355, doi:10.1038/nature03379.

Page, D. P. (2007), Recent low-latitude freeze-thaw on Mars, *Icarus*, *189*, 83–117, doi:10.1016/j.icarus.2007.01.005.

Peeples, W. J., W. R. Sill, T. W. May, S. H. Ward, R. J. Phillips, R. L. Jordan, E. A. Abbott, and T. J. Killpack (1978), Orbital radar evidence for lunar subsurface layering in Maria Serenitatis and Crisium, *J. Geophys. Res.*, *83*, 3459–3468, doi:10.1029/JB083iB07p03459.

Plescia, J. B. (1990), Recent flood lavas in the Elysium region of Mars, *Icarus*, *88*, 465–490, doi:10.1016/0019-1035(90)90095-Q.

Plescia, J. B. (1993), Wrinkle ridges of Arcadia Planttia, Mars, *J. Geophys. Res.*, *98*, 15,049–15,059, doi:10.1029/93JE01324.

Porcello, L. J., R. L. Jordan, J. S. Zelenka, G. F. Adams, R. J. Phillips, W. E. Brown, S. H. Brown, and P. L. Jackson (1974), The Apollo lunar sounder radar system, *Proc. IEEE*, *62*, 769–783, doi:10.1109/PROC.1974.9517.

Putzig, N. E., M. T. Mellon, K. A. Kretke, and R. E. Arvidson (2005), Global thermal inertia and surface properties of Mars from the MGS mapping mission, *Icarus*, *173*, 325–341, doi:10.1016/j.icarus.2004.08.017.

Ruff, S. W., and P. R. Christensen (2002), Bright and dark regions on Mars: Particle size and mineralogical characteristics based on Thermal Emission Spectrometer data, *J. Geophys. Res.*, *107*(E12), 5127, doi:10.1029/2001JE001580.

Seu, R., et al. (2007a), Accumulation and erosion of Mars' south polar layered deposits, *Science*, *317*, 1715–1718, doi:10.1126/science.1144120.

Seu, R., et al. (2007b), SHARAD sounding radar on the Mars Reconnaissance Orbiter, *J. Geophys. Res.*, *112*, E05S05, doi:10.1029/2006JE002745.

Smith, D. E., et al. (2001), Mars Orbiter Laser Altimeter: Experiment summary after the first year of global mapping of Mars, *J. Geophys. Res.*, *106*, 23,689–23,722, doi:10.1029/2000JE001364.

Tanaka, K. L., and D. H. Scott (1987), Geologic map of the polar regions on Mars, *U. S. Geol. Surv. Misc. Invest. Map, I-1802-C*.

Tanaka, K. L., J. A. Skinner, and T. M. Hare (2005), Geologic map of the northern plains of Mars, *U. S. Geol. Surv. Sci. Invest. Map, 2888*.

Ulaby, F. T., R. K. Moore, and A. K. Fung (1982), *Microwave Remote Sensing*, Addison-Wesley, Reading, Mass.

Ulaby, F. T., et al. (1988), Microwave dielectric spectrum of rocks, *Rep. 23817-1-TU*, Radiat. Lab., Univ. of Mich., Ann Arbor, Mich.

Watters, T. R., et al. (2007), Radar sounding of the Medusae Fossae Formation Mars: Equatorial ice or dry, low-density deposits?, *Science*, *318*, 1125–1128, doi:10.1126/science.1148112.

D. Biccari and R. Seu, INFOCOM, University of Rome "La Sapienza," Via Eudossiana 18, I-00184 Rome, Italy.

B. Campbell and L. Carter, Center for Earth and Planetary Studies, Smithsonian Institution, MRC 315, P.O. Box 37012, Washington, DC 20013-7012, USA. (campbellb@si.edu)

A. Egan, R. Phillips, and N. Putzig, Southwest Research Institute, 1050 Walnut Street, Boulder, CO 80302, USA.

R. Orosei, Istituto di Astrofisica Spaziale e Fisica Cosmica, I-00133, Rome, Italy.

J. Plaut and A. Safaeinili, Jet Propulsion Laboratory, 4800 Oak Grove Drive, Pasadena, CA 91109, USA.